https://ntrs.nasa.gov/search.jsp?R=19670002490 2020-03-24T02:41:03+00:00Z

NATIONAL AERONAUTICS AND SPACE ADMINISTRATION

Technical Report No. 32-981

JPL Fission-Electric Cell Experiment

W. F. Krieve

GPO PRICE $ _____

CFSTI PRICE(S) $ _____

Hard copy (HC) 1.00

Microfiche (MF) .50

ff 653 July 65

N67 11819

(ACCESSION NUMBER) 94 (PAGES) CR-79940 (NASA CR OR TMX OR AD NUMBER)

(THRU) 1 (CODE) 22 [redacted] (CATEGORY)

FACILITY FORM 602

JET PROPULSION LABORATORY
CALIFORNIA INSTITUTE OF TECHNOLOGY
PASADENA, CALIFORNIA

November 15, 1966

NATIONAL AERONAUTICS AND SPACE ADMINISTRATION

Technical Report No. 32-981

JPL Fission-Electric Cell Experiment

W. F. Krieve

Approved by:

Robert J. Mackin, *Manager,*
Physics Section

JET PROPULSION LABORATORY
CALIFORNIA INSTITUTE OF TECHNOLOGY
PASADENA, CALIFORNIA

November 15, 1966

Copyright © 1966
Jet Propulsion Laboratory
California Institute of Technology

Prepared Under Contract No. NAS 7-100
National Aeronautics & Space Administration

CONTENTS

FIGURES

N67-11819

ABSTRACT

A series of experiments was performed with two different large concentric cylinder fission-electric cells in thermal neutron fluxes up to 10^{10} n/cm^2 sec at the General Electric Nuclear Test Reactor. A clear-cut demonstration of the fission-electric cell concept was achieved. Fission fragment currents up to 10^{-8} amp, which were in good agreement with calculated values, were observed. Magnetic field suppression of electron counter-currents was completely successful. Electrostatic grid suppression of the extraneous electrons was much less effective.

The original cell configuration, in which the anode cylinder surrounded the inner cathode cylinder, achieved stable potentials of approximately one kilovolt. The modified configuration, in which the cathode with electron sweep rings surrounded the anode, reached potentials as great as 21 kv, but was not stable above 4 kv. Author

I. INTRODUCTION

A series of experiments was performed with a large fission-electric cell assembly to determine the operating characteristics and the limitations of such devices. A fission-electric cell, which would serve as a fuel element of a novel reactor, is a device for converting the kinetic energy of fission fragments directly into electrical energy (Refs. 1–6). It consists of a cathode which is covered with a thin layer of fissionable material and is the source of the charged fragments, an anode which serves as the collector of the charged fission fragments, and a charge separation mechanism. When the cell is irradiated with neutrons, fissioning of the material on the cathode occurs. A fraction of the fission fragments emerges from the fuel layer on the cathode and can be collected on a suitably positioned anode. As the fragments emerge from the fuel surface, they are accompanied by a large number of follow-out or δ electrons (Ref. 7). Because the momentum and kinetic energy of fragments are large compared with those of electrons, it is possible to return the electrons to their origin on the cathode with either a magnetic field or an electrostatic grid without affecting the fragment current.

Although fission fragments are born with large kinetic energy, their large mass and charge result in their having a short range in solid material (Ref. 8); the range of a fission fragment in UO_2 is approximately 10 mg/cm^2. This means that the layer of fissionable material on the cathode must be thin. It is also necessary that the cathode and anode be separated by a vacuum gap. Because of the large ratio between the kinetic energy and the charge of the fission fragments, the fission-electric cell is a high-voltage, low-current device.

For the device to function, it is necessary that the electron-suppression mechanism be capable of returning

the follow-out electrons to the cathode against the potential developed between the electrodes, in addition to the initial kinetic energy of the electrons. Initial kinetic energy of the follow-out electrons can be calculated from the mass and kinetic energy of the fission fragments. A mass 95 fission fragment with 100-Mev kinetic energy is capable of producing a δ electron of twice the velocity of the fragment, or approximately 2260 ev. Maximum voltage capability of the device can be calculated from the charge and kinetic energy of the fission fragments. A mass 95, 100-Mev fragment has an electronic charge of +20 to +21 during at least the first half of its range (Refs. 8, 9). Open-circuit potential with adequate electron suppression would thus be in the range of 4.7 to 5.0 million volts. A mass 138 fragment has a kinetic energy of approximately 60 Mev and an average electronic charge of +22. Because fission fragments are born with an isotropic distribution and a fraction of their energy is lost in traversing the finite layer thickness required for an operating device, optimum efficiencies of a fission-electric cell device are in the range of 1.0 to 2.0 million volts (Ref. 4).

The experiments to be described constituted the final phase of an analytical and experimental fission-electric cell program carried out by the Jet Propulsion Laboratory (JPL) in the period 1960–1964. Reference 5 gives a review of the fission cell reactor concept, its potential advantages for large-scale space power, and a 1963 view of the crucial problems and experiments to investigate them.

The JPL experimental program was carried out in three phases. The first, conducted in collaboration with G. Safonov, led to the demonstration that a potential could be developed by a simple fission cell configuration exposed to a neutron flux. The second phase involved immersion of prototype cells in the intense neutron fluxes of a reactor core for extended periods of time. This phase, described briefly in Ref. 5 and reported in detail in Ref. 6, was directed toward revealing any fundamental problems associated with material limitations. It culminated in the successful development of cells that survived intact through several per cent of fuel burnup and showed no important degradation of performance.

The final experimental phase, reported here, was directed mainly toward the phenomena limiting the achievable voltage. As presently conceived, the fission cell, to have a significant efficiency, must develop a potential gradient comparable to the best ever achieved across a vacuum gap—while positioned in an intense radiation field. This report describes our progress toward that goal.

The practical systems problems of a fission-electric cell reactor (plus radiation) employed for multi-megawatt space power have been treated at some length in an extensive analysis by D. J. Motski.[1]

[1]This work is reported in *Fluid Systems Design Concept For a Large Gas-Cooled Fission-Electric Cell Reactor Space Power Plant*, Technical Memorandum No. 33-283, Jet Propulsion Laboratory, Pasadena, California, to be published.

II. DESIGN CRITERIA

Design of the experimental apparatus for the final phase of the experimental program was based on the data and experience accumulated in the course of earlier fission-electric cell capsule experiments (Refs. 5, 6). It was realized that a crucial question in determining the potential usefulness of the fission-electric principle was the limitation of the achievable high voltage in a cell of a given dimension in a radiation field. It was also necessary to eliminate the end-effects observed in the capsule experiments because of the short cell lengths that were dictated by space and handling requirements. Visual inspection of the capsules after irradiation had indicated that a large quantity of anode material was deposited on the cathode. If this material had become ionized during the process of moving from anode to cathode, it would represent a source of internal leakage current that would limit cell performance. Also, results of the capsule experiments indicated that the quality of the vacuum in the interspace between electrodes had a large effect on the voltage capability of the capsules. Residual condensable gases could be removed by equipping the cell with greater pumping capacity; how-

ever, interspace gas resulting from the accumulation of sputtered electrode material could be minimized only by reshaping electrode surfaces.

Any attempt to reduce sputtering of fuel material from the cathode would also proportionately reduce the number of fragments leaving the cathode; thus, the control of sputtered material would have to be attempted at the anode. End effects could be minimized by ensuring that all fragments leaving the cathode would be capable of reaching the anode. This could be accomplished by a collimator that allowed only fragments with the proper energy and angle to leave the cathode.

The problem of a feed-through insulator in a radiation field could be circumvented by placing the insulator as far removed from the ionizing radiation as possible, with a vacuum lead between the fissioning and collecting region and the insulator. Because this problem was considered to be less important at this stage of development than that of the vacuum gap between the electrodes, the problem was eliminated from these experiments.

These conditions defined the overall cell design and the type of reactor that could be used for irradiation of the cell.

III. ORIGINAL CELL DESIGN

A. Cathode Design

The cathode used in the first series of tests is shown in Fig. 1. The basic cathode support, exclusive of base flange, was 28 in. long and 1.0 in. in diameter and was fabricated of 6061-T6 aluminum. Fuel in the form of fully enriched UO_2 was plated on six 2-in.-long spools that slipped over the cathode support. These spools were fabricated of Ti-75 titanium and had a wall thickness of 0.015 in. and an end rib 0.062 in. thick by 0.050 in. wide. One of the end spools had a rib at each end, to support the mechanical collimator. The fueled spools can be seen in Fig. 1. The dark area seen through the grid and collimator is the UO_2.

A total of 0.874 g of UO_2 was plated on the fuel elements; the uranium had an enrichment of 93.15% as U^{235}. The total plated area of the elements was 212 cm^2. This gave an average fuel element thickness of 4.1 mg/cm^2, or approximately 40% of a fragment range. The titanium spools were zincated before the uranium dioxide was plated. Zincating was accomplished

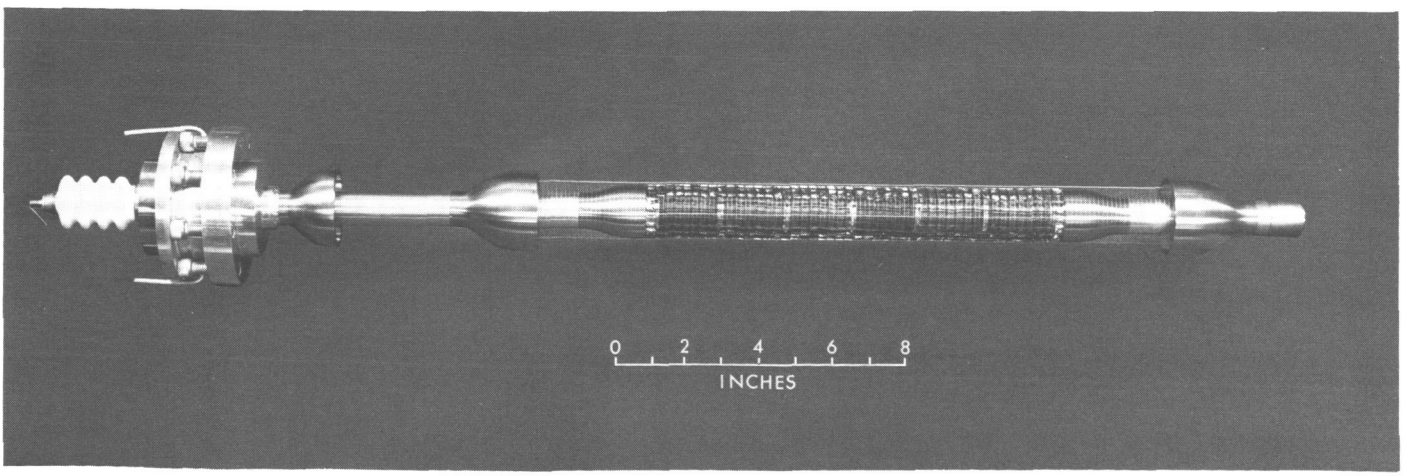

Fig. 1. Cathode assembly of original cell

by first cleaning the exterior surface of the spool with steel wool (fine) and then dipping the spool in a solution of 200 cc of concentrated nitric acid and 20 cc of hydrofluoric acid in enough water to make a liter. Following the acid dip, the spools were rinsed with distilled water and placed in an activator solution for a period of approximately 30 seconds. The activator solution contained 160 cc of concentrated phosphoric acid (H_3PO_4) and 100 g of ammonium bifluoride ($NH_4F \cdot HF$) in sufficient distilled water to make one liter of solution. After activation and a rinse in distilled water, the spools were placed in the zincate solution, which was maintained at 140°F. The zincate solution contained 525 g of sodium hydroxide (NaOH) and 100 g of zinc oxide (ZnO) in sufficient water to make one liter of solution. Approximately 5 minutes was required for the zincating. The spools were rinsed with distilled water and methyl alcohol, and were then dried by heating to 150°C in vacuum.

The uranium dioxide was plated from aqueous solution using ammonium oxalate as the carrier and uranyl nitrate as the uranium source. The plating-bath temperature was maintained at 176°F. The plating solution was added to the container with the electrodes and removed at the end of the plating process while a potential was applied to the electrodes. When the potential was lost at any time during the plating process, the deposited uranium oxide washed off of the fuel element. Concentration of the ammonium oxalate in the plating bath was maintained at such a level that the electrode potential was 8.5 $\pm$ 0.5 v and the current was 0.10 amp/cm^2 of plated surface. Submerged areas on the fuel element spools or rings on which fuel was not desired were masked with a strippable latex paint. The plating anode was made of platinum gauze. During the plating process, the uranium was added to the plating bath in the form of a uranyl nitrate solution. The uranium was added (as UO_2) to the plating bath at the rate of 0.5 mg/cm^2 of plated surface at 20-min intervals. This schedule was maintained until the desired quantity had been added. Following the plating, the fuel elements were rinsed with methyl alcohol and then heated to 150°C in a vacuum for a period of one hour, to insure the removal of the plating salts and complete dehydration. The actual quantity of uranium on the elements was determined by weighing them before and after plating. Better adherence of the uranium dioxide to the titanium spools was obtained when they were zincated before the uranium plating.

The mechanical collimator that covered the fueled area of the cathode was designed to allow the escape of only those fragments with proper energy and angle to be able to overcome a 250-kv potential between the cathode and anode. Openings in the mechanical collimator were ¼-in. square, and the width of the webbing was 3/16 in. The webbing was made of 0.0012-in.-thick Ti-75 titanium and was assembled by spot welding.[2]

Attached to either end of the collimator were end bells that tapered from the outer diameter of the collimator to the outer diameter of the cathode support. These were for support of the collimator and also for shaping the electrostatic field between it and the grid that covers the assembly.

The electrostatic grid was 1.87 in. in diameter and extended beyond the fueled region, so that the support insulators and shielding bells would be out of range of the emerging fragments. The grid was formed by spiraling a 0.005-in.-diameter titanium wire at a pitch of 8 turns per inch. Three axial 0.020-in. titanium wires extending the length of the grid acted as the support. The spiral wires were spot-welded to the axial wires at every crossover. Alumina discs supported the grid from the cathode support. The titanium bells that covered the insulators were to shield them from becoming contaminated with sputtered material that could cause arc-over when there was a potential on the grid. The grid lead extended through the center of the cathode support and terminated at the feed-through insulator on the base of the cathode support flange. Although the grid was sometimes used for charge separation, its primary purpose was to electrostatically screen the sharp edges of the mechanical collimator. During most of the cell operation it was grounded and served as the cathode surface.

The amplification factor of the electrostatic grid was estimated from the equation (Ref. 10):

$$\mu = \frac{2\pi n r_g \ln (r_a/r_g)}{\ln \coth 2\pi n R}$$

where

μ = amplification factor, the voltage between the cathode and anode (per volt on the grid) at which electron cutoff will occur

n = the reciprocal of the distance between the grid wires

r_g = radius of the grid

r_a = radius of the anode

R = radius of the grid wire

[2]By Kentucky Metals, Inc., Louisville, Kentucky.

Because of the dimensions of the cell, the planar equation gives similar results. For the planar case,

$$\mu = \frac{2\pi n (r_a - r_g)}{\ln \coth 2\pi nR}$$

Amplification factor of the grid was approximately 15. Before irradiation, it was possible to apply a potential of 10 kv to the grid without arcing or field emission.

B. Anode Design

The collector portion of the anode was fabricated of Ti-75 titanium. A shell of 0.0012-in.-thick sheet surrounded a cylinder of honeycomb material. The openings in the honeycomb material were 3/16 in. across flats and had a depth of 3/16 in. Thickness of the webbing material was 0.0012 in. The entire assembly was fabricated by spot welding.[2] An exterior view of the collector portion and the end bells (for field shaping and attaching to the anode lead) is shown in Fig. 2. The honeycomb material was used on the collecting surface of the anode to present a series of zero-potential cavities in which the fragments would be intercepted, in order that a large fraction of the neutral surface atoms sputtered by the fission fragments could be intercepted by the anode surface before they had a chance to reach a region where their becoming ionized would contribute to the internal leakage current of the cell. The collector surface was protected with a screen grid composed of 180 0.009-in.-diameter titanium wires suspended parallel to the surface (Fig. 3). The inside diameter of the screen grid was 4.10 in., and the outside diameter of the anode was 4.62 in. Overall length, including the end bells, was 32 in.

Thin material was used for the anode so that it would be essentially transparent to high-energy Compton and beta-decay electrons. It would also be a minimal source of these electrons and thus would decrease the contribution of nonfission events to cell current.

C. Overall Cell Design

The cell and vacuum envelope were designed so that the feed-through insulator would be outside the region of high radiation. Figure 4 shows the assembled cell ready for positioning in the reactor. The lower cylinder acted as a guard, surrounding the grid feed-through insulator. This cylinder, along with the grid lead from the power supply, could be pressurized with sulphur hexafluoride to reduce external leakage current in the

Fig. 2. Collector assembly of original cell

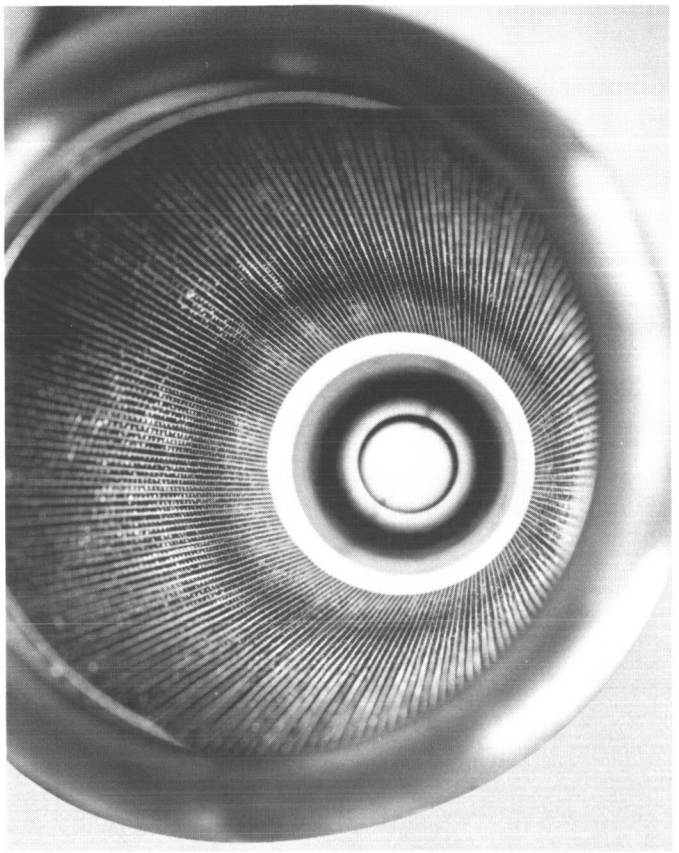

Fig. 3. Interior view of collector

grid circuit. The next section, the lower portion of the vacuum envelope, contained the cathode and anode centered in its interior. The outside diameter of the section was 6.10 in. and its wall thickness was 0.010 in. Total length from base to the centerline of its top flange was 42 in.

The section above, extending to the base of the large envelope and containing the juncture to which the ion pump was attached, constituted the upper vacuum envelope. It contained the anode lead, which extended from the collector portion of the anode to the lead section in the feed-through insulator. Outside diameter of the section was 4.25 in., and the wall thickness was 0.125 in. Total length between the centerline of the two terminal flanges was 38.25 in. The ion pump was connected to this section through a 90-deg ell of Type 304 stainless steel.

The feed-through insulator was located in the large envelope section. Figure 5 is a view of the insulator with terminal dome, flange covers, and corona ring in place. The diameter of the anode lead within the insulator

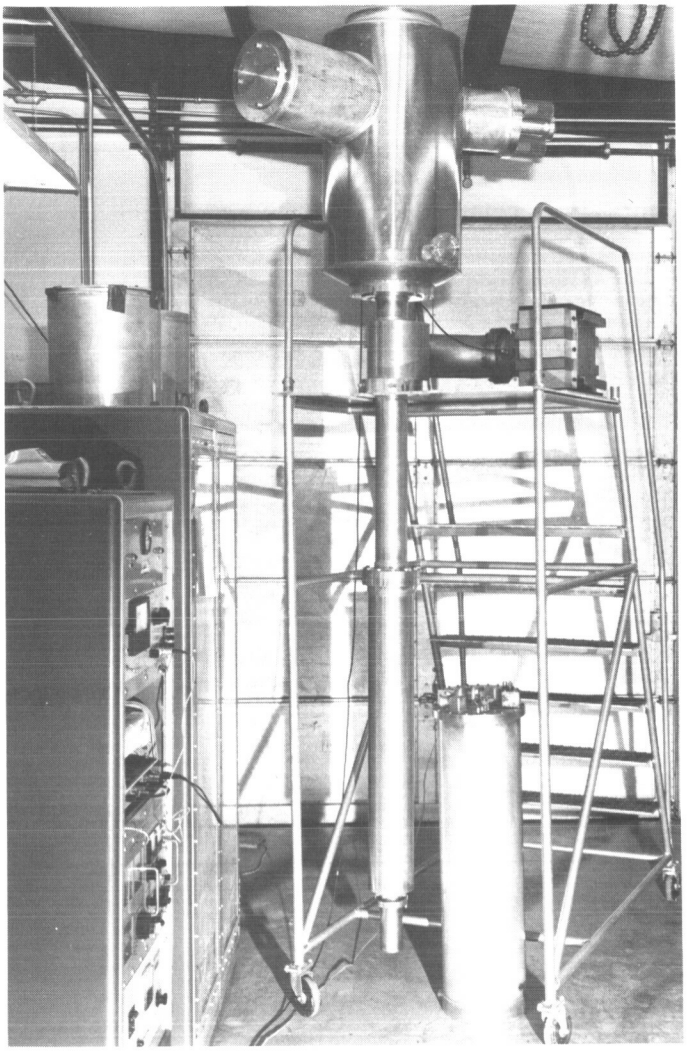

Fig. 4. Assembled cell ready for positioning in reactor

section varied as an exponential horn. It had the same diameter as the inside of the insulator at the high-voltage end and decreased to the anode lead diameter of 1.47 in. at the base of the insulator. The insulator, which formed the top portion of the cell vacuum envelope, had an inside diameter of 4.2 in. and a wall thickness of 0.2 in. The outside diameter of the terminal dome, the flange covers, and the corona rings was 7.87 in. Overall length of the ceramic portion of the insulator was 18 in. The insulating material was a high alumina ceramic. Vacuum seal was made to the stainless steel (304) flanges at either end by heli-arc welding to a Kovar metal lip that was oven brazed to the ceramic.[3]

The large upper envelope surrounding the insulator could be either pressurized or evacuated during opera-

[3]By Ceramaseal, Inc., New Lebanon Center, New York.

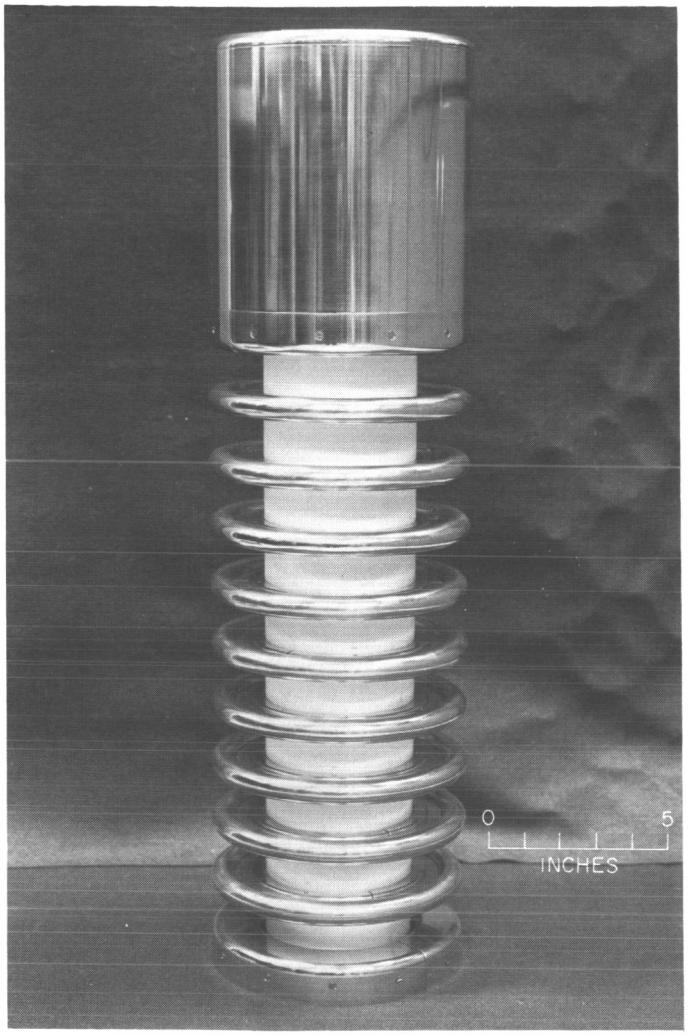

Fig. 5. Anode feed-through insulator

tion. One of the large upper side arms contained the generating voltmeter for measuring cell potential. The other upper side arm provided access for a lead cable for measuring cell currents under short-circuit conditions or with resistors in the circuit. The side arm could also be used for connection of an ion pump for evacuation of the envelope. Under this condition, the generating voltmeter was used to measure open-circuit potentials. The lower side arm was used for rough pumping before starting the ion pump. Outside diameter of the envelope was 18.25 in. and the wall thickness was 0.125 in. Total length was 36 in.

All parts of the cell envelope, with a few exceptions, were made of 6061-T6 aluminum. The exceptions were (1) the flanges on the insulators, the ell and its flanges, and the ion pump, which were made of 304 stainless steel, and (2) the anode and cathode, which were made of titanium. All flange seals that formed closures for the basic cell (with the exception of the one on the ion pump) were made with stainless steel O-rings. These O-rings were formed from stainless steel tubing butt-welded to form the closed ring and then silver-plated.[4] O-ring groove bases and the other mating surfaces had an 8 to 16 AA finish. No problems were encountered in obtaining helium-leak-tight seals. The leak detector used had a sensitivity of 2×10^{-10} atm-cc/sec-division. The ion-pump seal used a crush copper gasket. Flange seals on the insulator envelope and the grid shield were made with Viton O-rings.

The ion pumps used were ULTEK Model 20-092, with 100-liter/sec pumping capacity.

D. Materials Selection

Titanium structural members and surfaces were used in regions of high radiation intensity and in areas where the fragments would be intercepted. The reasons for the choice of titanium were:

1. High melting point, which would reduce the amount of sublimation if parts became overheated;
2. Low density, which would result in minimum production of Compton electrons due to interaction with gamma rays;
3. Very low activation cross section leading to beta decay, which would contribute to cell background current;
4. Low secondary electron production per incident primary electron (Ref. 11); and
5. Low number of sputtered atoms per incident high-energy impacting ion (Ref. 12).

Aluminum was used for the basic structure of the cell because of its machinability and weldability. It also has the required low density and small activation cross section for beta decay. Its total neutron cross section is small, thus minimizing the thermal neutron flux perturbation due to structural material.

E. Field Coil Design

The magnetic field for electron suppression was supplied by a solenoid that surrounded the lower vacuum envelope, Fig. 6. The assembly consisted of four separate coils of two windings each, canned in a watertight container. Two of the coils were 36 in. long, and each of

[4]By United Aircraft Products, Inc., Dayton, Ohio.

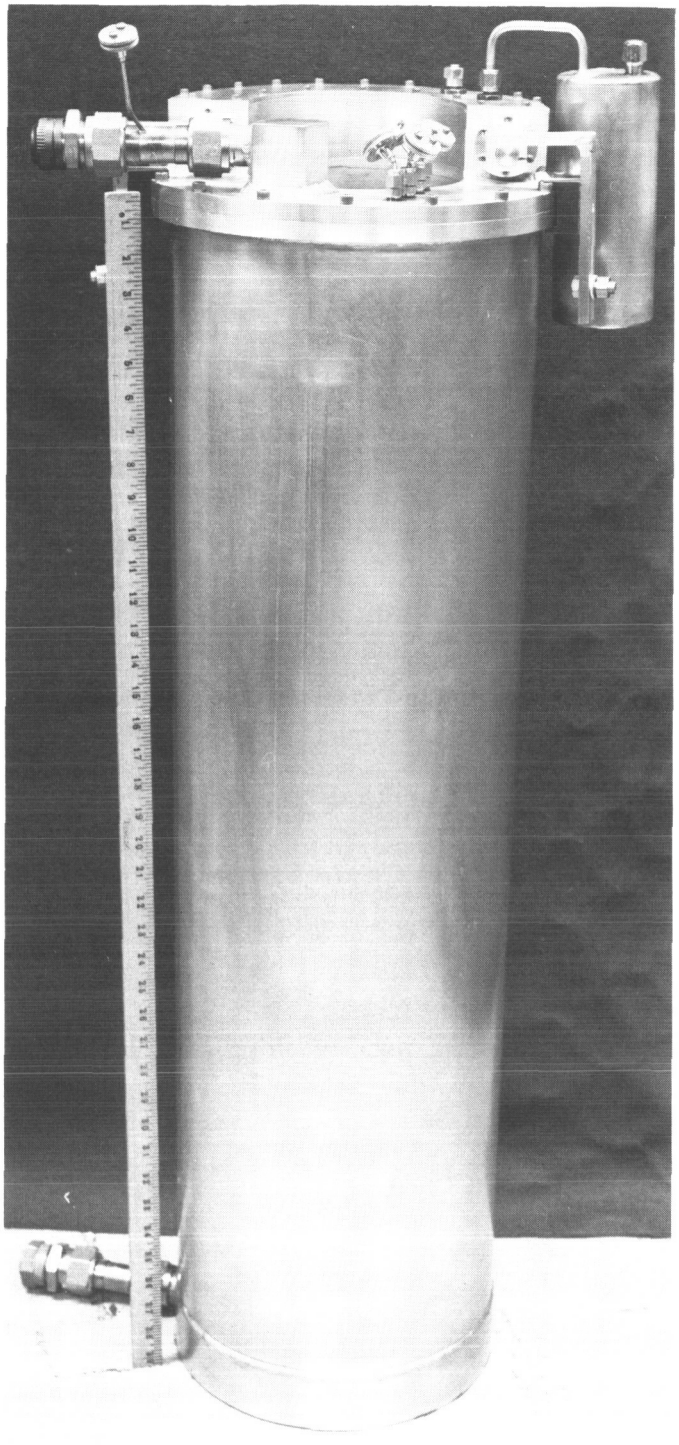

Fig. 6. Magnetic field coil

the other two was made up of two 1-ft sections separated by a 1-ft void. This was done to produce a magnetic bottle that would enclose the active region of the cell. The coils were enclosed in a water jacket and were separated from each other by a coolant passage. Teflon was used as the insulating material between windings and between the windings and the can. The remaining void space and the terminal box at the top of the assembly were filled with silicone oil. A surge tank was provided (Fig. 6) for expansion of the oil during operation. Each long coil was paired with one short set in series and the two resulting sets were connected in parallel. Resistance of the combination was 1.5 ohms at room temperature and 2.5 ohms at the maximum operating temperature. The power supply used with the field coil had a rated output of 140 amp at 350 v. A calibration of the centerline axial magnetic flux is shown in Fig. 7.

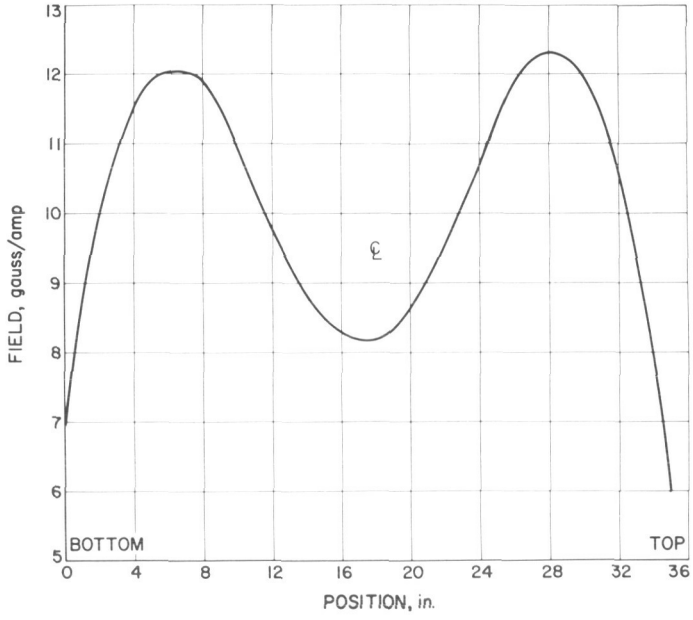

Fig. 7. Centerline axial magnetic flux

The windings, the coil canning material, and the cooling jacket of the field coil were made of 6061-T6 aluminum. A primary loop heat exchanger was provided for cooling the field coil. Separation of the coolant streams was necessary to avoid any possible contamination of coolant that was to be dumped.

The magnetron equation used to determine the maximum potential capability of the cell as a function of magnetic field was the one in Ref. 13, modified by the inclusion of an initial electron kinetic energy term:

$$N = 2\pi r_a \left(\frac{V + V_e}{300}\right)\left(\frac{2m_0c^2/e}{V + V_e} + 1\right)^{1/2}$$

$$- 2\pi r_c \left(\frac{V_e}{300}\right)\left(\frac{2m_0c^2/e}{V_e} + 1\right)^{1/2}$$

where

N = the total number of maxwells between the cathodes and anode

r_a = radius of the anode, cm

r_c = radius of the cathode, cm

V = potential between the cathode and anode, volts

V_e = initial kinetic energy of the electrons, volts

m_0c^2/e = rest mass energy of an electron, volts

F. Monitoring Equipment

Current output from the cell was measured with a Hewlett-Packard Model 425-AR Microvoltampmeter during the first series of tests, and, in addition, with a Cary Model 31 Vibrating Reed Electrometer during the subsequent tests. Voltage buildup was monitored by measuring the output current from the cell with various resistances in series with the anode circuit. The resistor stacks used (Fig. 8) had values of 10^{12}, 10^{13}, 10^{14}, and 10^{15} ohms and were installed in load boxes that were maintained at a slight overpressure of sulphur hexafluoride (SF_6). During these measurements the insulator envelope was also under a slight pressure of SF_6.

Open-circuit potentials could be measured with the generating voltmeter, Fig. 9. Although a generating voltmeter is considered a null instrument, the 3×10^{-11} amp drawn by this unit was not insignificant. The meter was completely enclosed, and the drive employed a magnetic coupling through an aluminum window. Driving speed of the voltmeter was either 360 or 450 rpm, the lower speed being used to minimize the current drawn by the instrument. Difficulties were encountered with the lower speed, but 450-rpm operation proved trouble-free. Null-point voltages were determined with a Hewlett-Packard Model 400-H AC Vacuum-Tube Voltmeter.

G. Cell Evacuation

The cell was rough-pumped through a ¾-in.-diameter aluminum tube in the top cover cap of the feed-through insulator, using a Welch Duo-Seal pump connected to the cell through a glass cold trap immersed in liquid nitrogen. After the cell was rough-pumped and the ion pump fired, the cell was isolated from the initial pump-down system by a cold-weld pinch-off of the aluminum tube in the top cover cap. The top cover cap and the tube stub were under the terminal dome of the feed-through insulator (Fig. 5). The assembled cell was baked

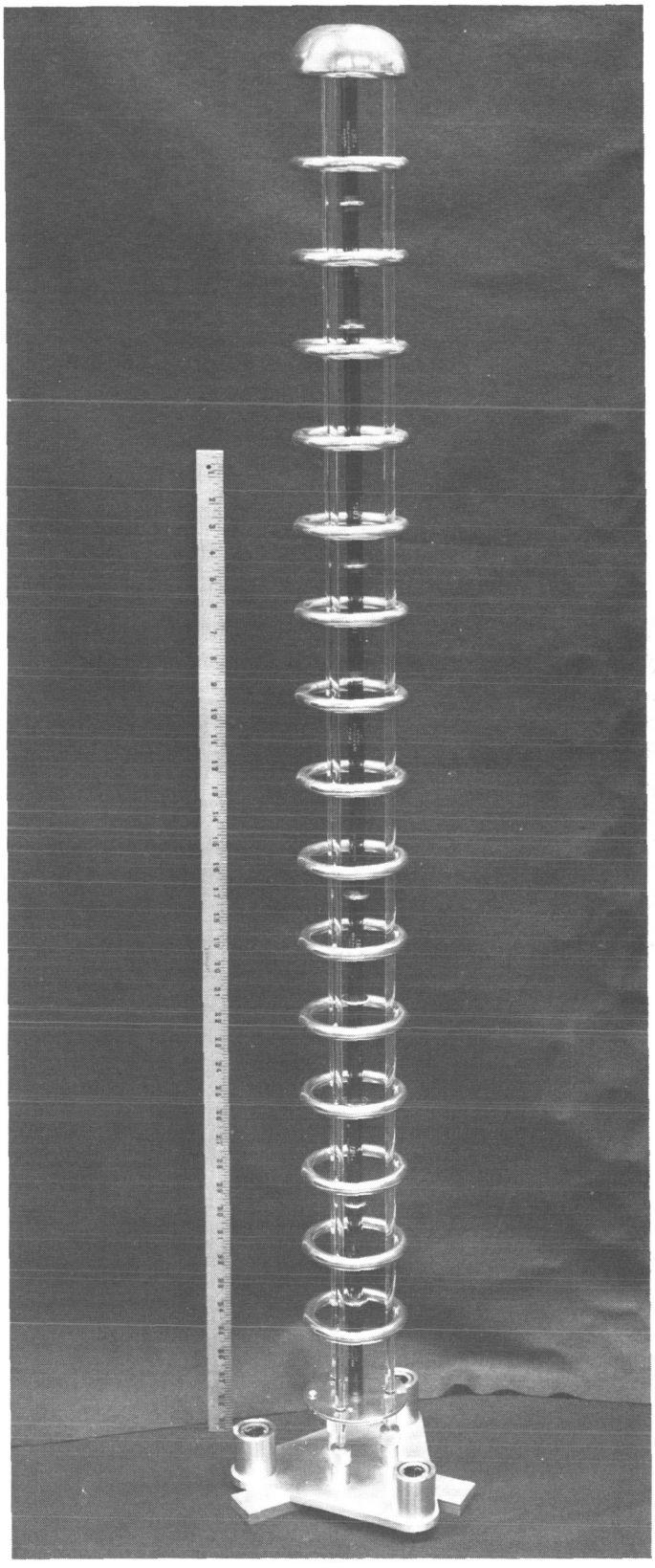

Fig. 8. Resistor stacks for load resistance

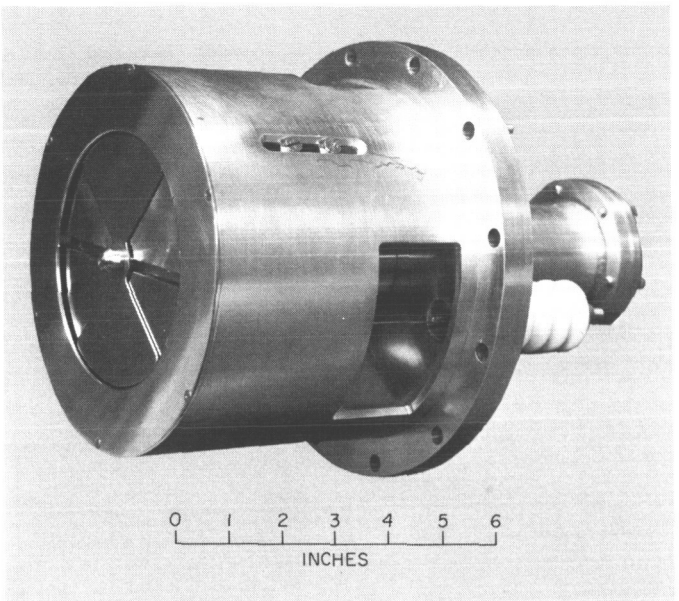

Fig. 9. Generating voltmeter

out at temperatures between 125 and 150°C, using eight 250-w heat lamps. The cell was pumped for 2 weeks at the elevated temperature before being positioned in the reactor. Cell pressure prior to irradiation was between 3×10^{-9} and 5×10^{-9} mm Hg.

H. Reactor

The cell was irradiated in the General Electric Nuclear Test Reactor, Vallecitos, California. The reactor has an annular core, 18 in. in diameter by 18 in. long, in a graphite cube that is 5 ft on a side. The cell was positioned along one of the vertical graphite faces, in line with the centerline of the core. The ion pump rested on a 1-ft-thick concrete shield that covered the reactor assembly. Reactor power level could be varied from 0.02 w to 30 kw. Thermal neutron flux at the centerline of the cell (with the cell in place) was 10^{10} n/cm^2-sec at a reactor power level of 30 kw. The accompanying gamma dose rate was approximately 5×10^4 r/hr. Gamma dose rate at the feed-through insulator was 16 r/hr at a power level of 30 kw.

IV. EXPERIMENTAL DATA FROM ORIGINAL CELL

A. Short-Circuit Current

At a reactor power level of 30 kw, the short-circuit current with no electron suppression was -1.5×10^{-7} amp; with magnetic-field suppression, it was $+1.1 \times 10^{-8}$ amp. Calculated and experimental field current for complete turnaround of the follow-out electrons was 9.4 amp. This corresponded to electrons with a maximum initial kinetic energy of 2300 ev.

A positive current indicated a net flow of positive charges from the cathode to the anode, and a negative current indicated a net flow of electrons.

There were problems in determining the reactor power level for levels below 30 kw because of instrument limitations. At a nominal power level of 1 kw, during the initial stages of cell irradiation, the anode current was

-7.75×10^{-9} amp with no electron suppression and $+2.18 \times 10^{-10}$ amp with magnetic field. The maximum current with -1250-v grid suppression was $+1.6 \times 10^{-10}$ amp. Anode current was maximized with grid potential at this value. Figures 10 and 11 are plots of the output current as a function of magnetic field strength and electrostatic grid potential.

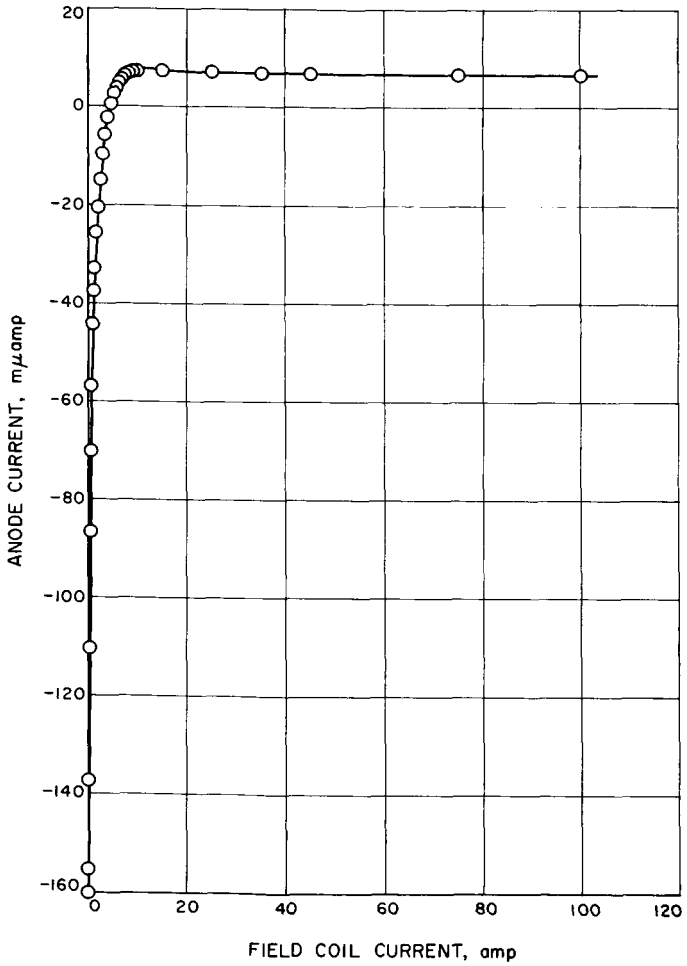

Fig. 10. Short-circuit current as a function of magnetic field strength, original cell. Reactor at 30 kw

The cell current without electron suppression decreased with accumulated irradiation. This was apparently due both to vacuum cleanup of the anode and cathode surfaces and to accumulation of uranium on the anode. Current with magnetic field suppression remained constant within the reproducibility of reactor power level.

Current readings both with and without electron suppression were positive immediately after subjecting the

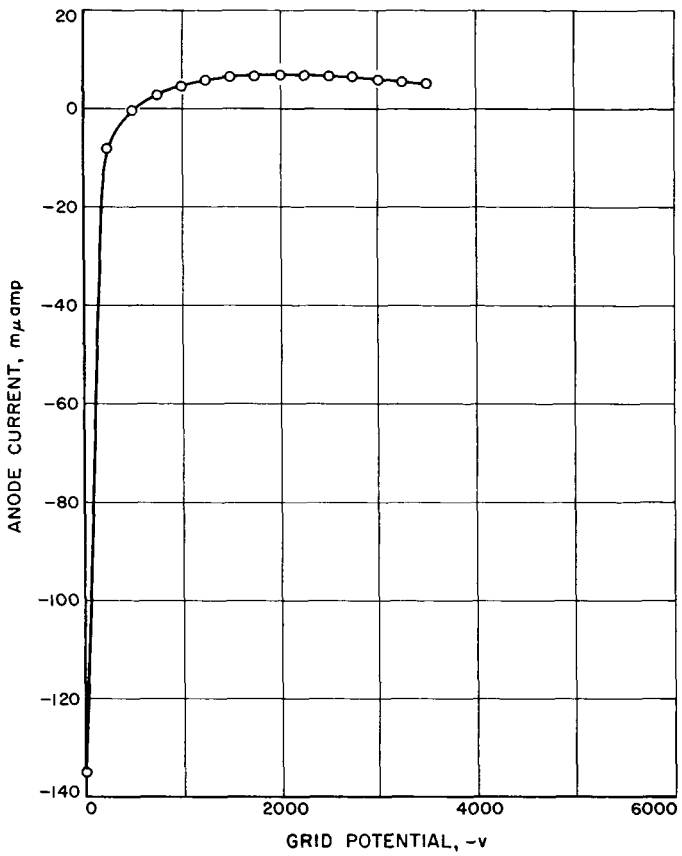

Fig. 11. Short-circuit current as a function of electrostatic grid potential, original cell. Reactor at 30 kw

cell to glow-discharging. This condition persisted up to several hours after the glow ended, probably because of static charge buildup on the corona rings of the feedthrough insulator and the anode lead. The cell was glow-discharged periodically for vacuum cleanup of the electrode surfaces. Glow discharge was sustained by applying a potential to the anode with the magnetic field energized. Various combinations of magnetic field and anode potential were used.

B. Leakage Current Tests

A series of leakage current tests was performed with various voltages applied to the anode and with various magnetic fields. These tests were performed at a constant reactor power. Applied potentials were in the range of 25 to 45 kv. The leakage current with no magnetic field and with the grid grounded was higher than the measured short-circuit current of the cell. This condition probably resulted from amplification of the electron current through outgassing and ionization within the cell and from sweepout of electrons and ions in the insulator

envelope. As the magnetic field strength was increased, the leakage current would decrease and approach a minimum value. The approach to the minimum value would be interrupted when current in the range of 23 to 25 amp was applied to the field coil independent of the applied potential. In this current range, the cell would start to break into glow discharge. It was possible to increase the magnetic field at a moderate rate through this region and avoid having a glow discharge condition. The leakage current would return to the minimal value at field currents above 25 amp. Minimum leakage current would be reached at a value of the field slightly less than that calculated for complete turnaround of the follow-out electrons. A slight increase in magnetic field at this condition would cause an increase in leakage current approximately three orders of magnitude over the short-circuit fragment current. Further increase in magnetic field would result in glow discharge. Figure 12 is a plot of relative leakage current as a function of magnetic field.

For all tests of this type, the potential applied to the anode had to be greater than 23 kv; otherwise, the cell would break into glow discharge at magnetic fields well below the magnetron limit.

The higher leakage currents from the cell were measured on the 0- to 20-μamp meter of the power supply. The lower leakage currents were estimated by comparing voltage leak-off rates from the cell. The cell was precharged to the desired voltage, and the current through the 10^{14}-ohm resistor stack connected to the anode lead was measured as a function of time. This was first done when the reactor was off and had been off for several days. These same measurements were then made with the reactor at power and with the desired magnetic field. A comparison of the leak-off rates under the two conditions gave an indication of the cell leakage current at reactor power conditions.

C. Maximum Cell Potential

The maximum potential generated by the first cell configuration was between 800 and 1000 v, as measured through the resistor stacks. The generating voltmeter indicated a potential of 880 v. These maximum potentials were achieved with 50 amp in the field coil. The electrostatic grid was ineffective for producing a potential buildup.

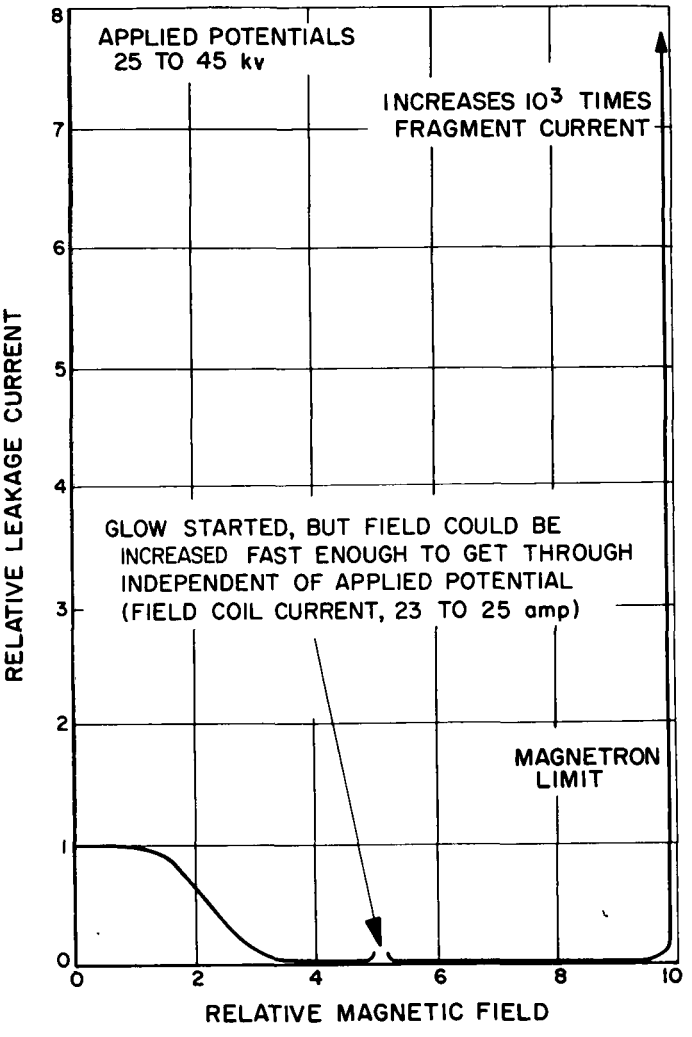

Fig. 12. Relative leakage current as a function of magnetic field, original cell

The first cell configuration was irradiated for two sets of experiments. The first set was terminated when it was concluded that the interior cell parts had been damaged while the cell was glow-discharged for vacuum and surface cleanup. Several wires of the screen grid on the anode had crossed, and the honeycomb material was exposed to the electrostatic gradient between the electrodes when a potential was applied to the anode. Field emission was noted at potentials above 8 kv. The second series of tests of this cell was performed after the repairs were made and the vacuum had recovered to the operational value.

V. REVISED DESIGN CRITERIA

Results from the first two series of tests with the initial cell configuration indicated that the large quantity of free electrons in the space between the electrodes may have been responsible for voltage limitation of the cell. It appeared from the data taken with applied anode potential and magnetic field that electrons were the charge carriers responsible for the internal leakage current. Although there was considerable difference in the size of the fission-electric cell and the fission-electric cell capsules (Ref. 6), their leakage current and voltage buildup behavior was essentially the same. It was concluded that electron trajectories in the two different cell types were approximately the same.

With magnetic field strengths sufficient to contain all or nearly all electrons, electron concentration in the interelectrode space may become quite large. The follow-out electrons accompanying the fission fragments constitute a very large source of electrons at the cathode surface. At magnetic field strengths equal to or larger than the magnetron limit of the anode potential, these electrons are returned to the cathode. Any energy loss process, such as an ionizing collision with a neutral atom, experienced by an electron would, however, keep the electron from returning to the cathode and it would eventually drift to the anode. An electron produced in the space between the electrodes through ionization would also eventually drift to the anode. The potential difference between the cathode and anode determines the region between the electrodes where the maximum number of ionizing collisions occurs. Maximum probability for ionizing collisions between electrons and most neutral atoms occurs for electron energies around 100 ev (Ref. 14). This means that at any appreciable cell potential the ionizing collisions would occur near the cathode. A large quantity of uncontrolled sputtered material is produced near the cathode by the emerging fragments. Ions produced in the region of a 100-v potential are capable of sputtering additional neutrals as they strike the cathode, thus increasing the material available for ionization. By this ionization process an internal shorting current could occur, and with applied anode potential it could develop into a glow discharge. The modified cell was designed to reduce the number of electrons accumulated between the electrodes and to reduce the average path-length of the electrons in order to avoid this occurrence.

VI. MODIFIED CELL DESIGN

In the modified cell (Fig. 13), the cathode surrounds the anode, and the fuel elements on the cathode are alternated with nonfueled rings that can be maintained at positive potentials with respect to the fuel elements. For a cell in which the cathode surrounds the anode, the path-length of the electrons originating at the cathode surface is considerably reduced in comparison with that in a cell that has the anode surrounding the cathode and has similar electrical characteristics at magnetron cutoff. The nonfueled elements act as sweep rings to remove those electrons from the inner space which have insufficient energy to reach the cathode surface. Except for the cathode and anode assembly, the cell was the same as in the previous experiments (Fig. 4). A metal valve,[5] utilizing an indium seat, was used for cell isolation following the rough pump-down and firing of the ion pump. This replaced the section that employed cold-weld pinch-off for isolation in the earlier experiments. Pump-down before firing the ion pump was done with a well-trapped oil-diffusion pump. Bake-out procedure was the same as that described above.

[5]Kane Engineering Laboratories, Palo Alto, California.

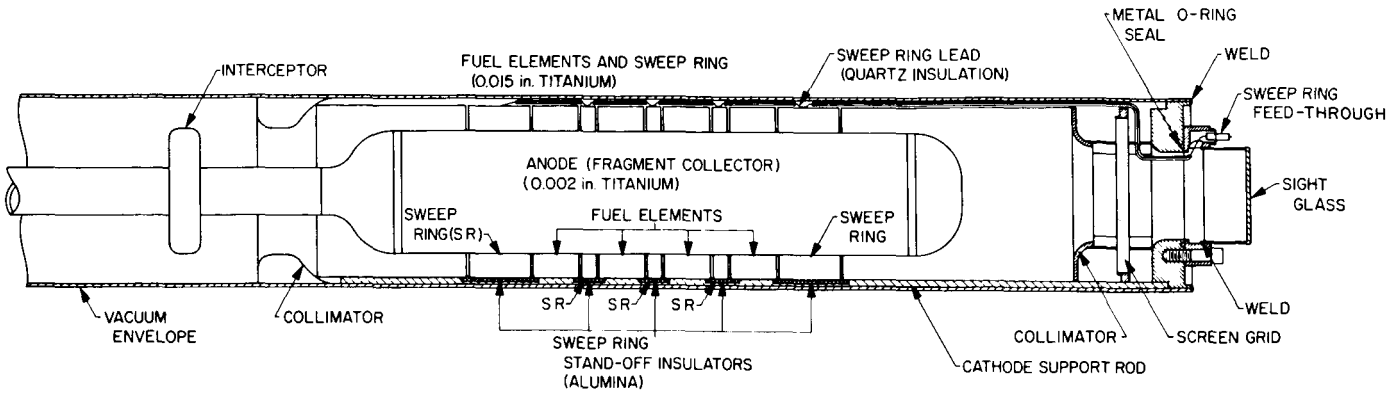

Fig. 13. Diagram of modified cell

A. Cathode Design

The cathode assembly was fitted into the cell vacuum envelope (Fig. 13). It consisted of the fragment collimators, the sweep rings and insulators, the fuel elements, the screen grid, the sight glass, and the feed-through insulator for the sweep rings. The collimators, sweep rings, fuel elements, and screen grid were supported on six titanium rods attached to a base flange. The base flange, which was aluminum (6061-T6), was welded to the vacuum envelope. The sight glass and feed-through insulator were welded into a stainless steel (304) flange bolted to the base flange; the seal was made with a silver-plated stainless steel O-ring. Both the feed-through insulator and the sight glass were bonded to Kovar metal, which was welded to the stainless steel flange. Overall length between the collimator extremes was 26¼ in.

Four individual fuel elements were used. Each had an inside diameter of 5.49 in., a thickness of 0.015 in., and a length of 1.50 in. The fuel-element rings were formed from titanium (Ti-75) sheet, closed by continuous spot welding.[2] The inner surface of the rings was zincated before plating with uranium dioxide. A 1/16-in.-wide strip at either end of the ring and six ⅛-in. strips corresponding to the positions of the support rods were devoid of uranium, to allow for handling the rings and for spot-welding them to the support rods. A total of 2.83 g of uranium dioxide was plated on the four fuel element rings, giving an average fuel element layer thickness of 4.83 mg $(UO_2)/cm^2$.

The sweep rings were made of the same material as the fuel elements and had the same inside diameter and wall thickness. The three rings that separated the fuel elements were each ½ in. wide, and the two rings that bounded the fueled region were each 2 in. wide. Alumina insulators fitted into slots in the support rods held the sweep rings in place and insulated them from ground. The sweep ring lead was a titanium wire sleeved with a quartz tube for electrical insulation. The rings were tied together electrically with three such leads, but only one extended to and was connected with the feed-through insulator. These electrical leads also served as mechanical supports for the rings. The sweep rings were separated from the fuel elements and from adjoining rings by 1/16-in. voids. A potential of 10 kv was applied to the sweep-ring assembly (in the absence of radiation) without electrical breakdown.

The upper collimator of the assembly was designed to intercept fragments that would miss the anode and strike the vacuum envelope in a region of little or no magnetic field. It was a titanium spinning with an average wall thickness of 0.020 in. and a minimum inside diameter of 4.00 in. The lower collimator was present to help produce a zero potential cavity in the lower part of the cell. No fragments were to be intercepted by it during operation. It, too, was a titanium spinning with a minimum diameter of 3.00 in. and a thickness of 0.125 in.

The region between the bounding sweep rings and the collimators was filled with aluminum (6061-T6) rings, with an inside diameter of 5.49 in. and a thickness of 0.015 in. The purpose of these rings was to shield the support rods and to present a continuous electrode surface.

Located between the lower collimator and the base flange was the screen grid. The purpose of this grid was

to complete the zero-potential cavity in the lower portion of the cell where fragments that missed the anode would be collected. Because of the finite length of the magnetic field coil, the secondary electrons produced by fragments collected in the lower portion of the cell would have large turnaround radii in the diminishing field. The zero-potential cavity would allow for a high probability of surface attachment of these electrons before they were influenced by the electrostatic field between the cathode and the anode. The grid was fabricated of 0.009-in.-diameter titanium wire on an aluminum support ring. Spacing between centerlines of the wires was 0.100 in. A center cross hair was established on the grid by angling wires from several directions. This cross hair, along with a center cross hair etched on the sight glass, was used for centering the anode.

The main purpose of the sight glass was to ensure centering of the anode during assembly of the cell. It was also used to observe any anode movement during the application of high voltage before irradiation. There was no detectable anode movement with potentials up to 50 kv. The position of the cell and the radiation intensity precluded observation of the cell during irradiation.

B. Anode Design

As in the original cell configuration, the anode was suspended from the feed-through insulator on a ring of six leveling screws. The thin-anode concept was retained in the design of this cell. The collector portion of the anode (Fig. 13) was fabricated of 0.002-in.-thick titanium sheet. The cylindrical section was closed by spot-welding an internal lip. The outside diameter of the collector portion of the anode was 3.90 in. Two aluminum discs, along with the two titanium adaptor rings at either end of the collector section, maintained its cylindrical shape. The assembly was held together by a 6-32 stainless steel threaded rod that extended between the adaptor rings through the center of the collector. The end bells were spot-welded to the adaptor rings. Overall length of the collector, including the end bells, was 21 in. The end bells were titanium spinnings 0.022 in. thick. All titanium used was Ti-75 or Ti-55.

The interceptor (Fig. 13) was an aluminum disc positioned on the anode lead above the cathode collimator. The purpose of the interceptor was to collect the fragments that had escaped interception by the anode collector and the cathode collimator. The interceptor had an outside diameter of 4.00 in. and a thickness of 0.75 in.

VII. EXPERIMENTAL DATA FROM MODIFIED CELL

A. Short-Circuit Current Measurements

The short-circuit currents measured as a function of magnetic field were somewhat different from those of the original cell configuration. The zero-field current was negative and the current became more negative as the field was increased. It reached a maximum negative value at 0.25 amp in the field coil and then became less negative and finally positive with increasing magnetic field (Fig. 14). The calculated field for complete turnaround of 2300-ev follow-out electrons for this cell was 9.8 amp. The 2300-ev energy was the value observed in the previous experiments with the anode surrounding the cathode. However, complete turnaround was not obtained until the field-coil current was 20 amp (Fig. 14). This discrepancy was probably due to end effects that were not accounted for.

The increasing negative value of output current with magnetic field was expected, since all the electrons produced by the fragments at the anode were intercepted by the cathode, while not all electrons originating at the cathode would reach the anode. The turnaround capability of the magnetic field would be greater for the electrons from the anode than for those from the cathode. Electron current from the anode would therefore be reduced at a more rapid rate and complete cutoff reached at a lower field.

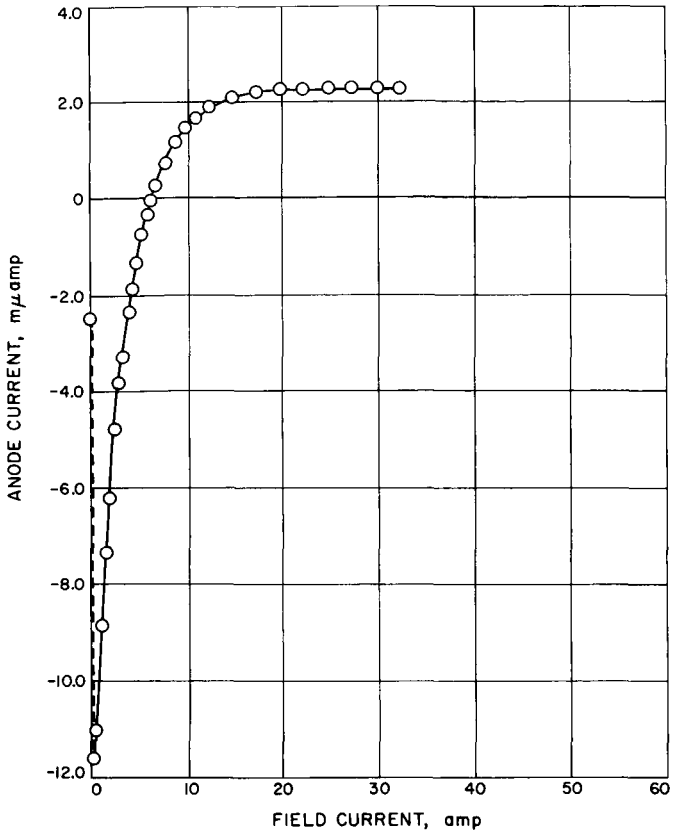

Fig. 14. Short-circuit current as a function of magnetic field strength, modified cell

Pressure in the cell vacuum envelope during this experiment, and also during succeeding experiments with irradiation, was in the range of 1×10^{-7} to 3×10^{-7} mm Hg.

B. Magnetic Field–Sweep Ring Combinations

A series of tests was made to determine the combination of applied anode potential, magnetic field strength, and sweep ring potentials that would result in a minimum anode leakage current under irradiation. The same value of minimum leakage current, 2.5 to 3.0 μamp, was obtained for several combinations of the variables. Optimum sweep-ring potentials were in the range of 2.25 to 3.0 kv. With magnetic field, a glow discharge would develop from the rings with potentials above 3.0 kv, and the rings were ineffective at potentials below 2.0 kv.

C. Leakage Current With No Electron Suppression

Anode leakage current without electron suppression appeared to be caused by two separate mechanisms, one prevailing at applied potentials below 2 kv, and the other becoming dominant above 2 kv (Fig. 15). The leakage current in the lower voltage range is probably internal to the cell and becomes saturated in the range of 2 kv. Leakage current above 2 kv was probably external to the cell and was apparently due to ionization of the gas in the insulator envelope.

D. Resistor Stack Data

The resistor stacks were connected to the output dome of the cell by a 17-ft lead of RG/220 coaxial cable. During the time that measurements were taken, the load box in which the resistor stacks were located and the insulator envelope that surrounded the anode feed-through were purged with SF_6. Measurements with the resistor stacks indicated a potential buildup of only a few hundred volts with the sweep rings grounded. Maximum indicated potential buildup was 1.3 kv with 2.5 kv applied to the sweep rings and with 40 amp in the field coil. All other combinations resulted in lower potential buildup.

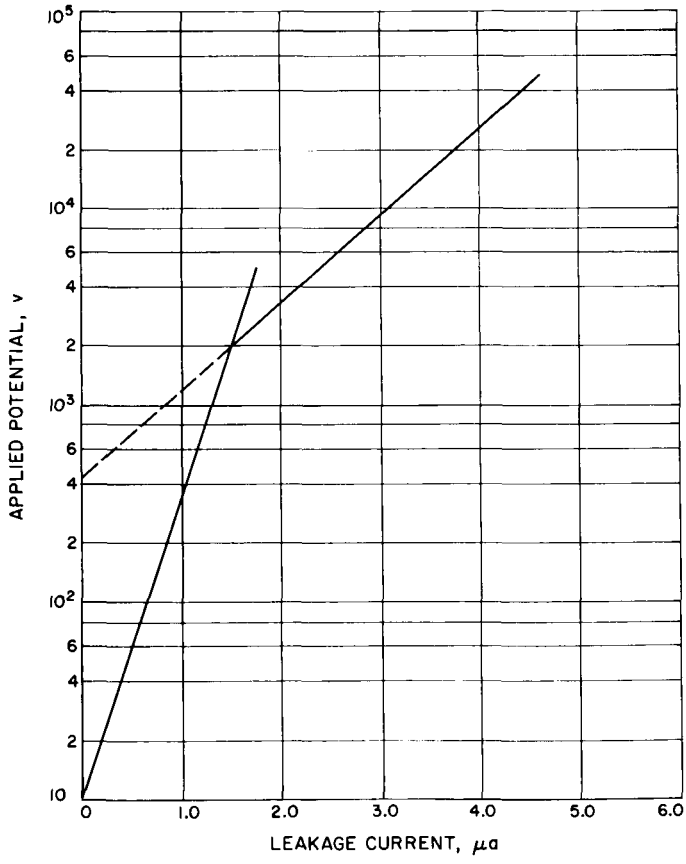

Fig. 15. Leakage current at zero magnetic field as a function of applied potential, modified cell. Reactor at 30 kw

During this series of tests, one leg of the field coil shorted to ground. This leg had to be removed from the circuit in order to proceed with the experiment. Removal of one of the legs of the coil did not change the axial magnetic field profile or the magnetic field strength with coil current. It did mean, however, that only one-half of the maximum current could be used, and thus one-half maximum field strength. The shorting of the coil was apparently caused by deterioration of the Teflon insulation of the windings by radiation damage.

E. Generating-Voltmeter Data

The generating voltmeter (Fig. 9) was positioned in the insulator envelope and looked at the output dome connected to the anode of the cell. The potential on the dome induced a potential on the pickup plates of the voltmeter. This induced an ac potential, because of the spinning vanes that alternately covered the pickup plates. A balance potential was then applied to a plate on the opposite side of the pickup plates from the dome. The spinning vanes alternately exposed the pickup plates to the dome and then to the balance plate. The potential applied to the balance plate could thus be used to null the ac output of the voltmeter. Nulling potentials were determined for various applied potentials on the dome; the calibration curve is shown in Fig. 16. The insulator envelope was under vacuum during the time that measurements were taken with the generating voltmeter. Pressure was in the range of 3×10^{-7} to 1×10^{-6} mm Hg during operation.

The results of the open-circuit tests with the generating voltmeter indicated that the cell could build up and maintain steady potentials with currents of 35 amp or less in the field coil. Potentials as large as 3.8 kv were achieved. With fields above 35 amp, cell operation was unsteady. The cell voltage repeatedly rose to a peak value, then fell to zero with the onset of a discharge. The recovery voltage following each discharge was 4000 $\pm$ 400 v, and was held for a period of a few seconds. From this level, the voltage again rose to its peak value and was almost immediately discharged once more. The value of the peak potentials reached in these cycles increased with increasing magnetic field. Maximum reproducible peak voltage at the 60-amp maximum field coil current was 13.5 kv. A maximum peak of 21 kv was once developed with 60 amp in the field; however, it was not reproducible. The potential on the sweep rings for these tests was 2.5 $\pm$ 0.25 kv. Figure 17 is a plot of the experimental data along with a series of magnetron

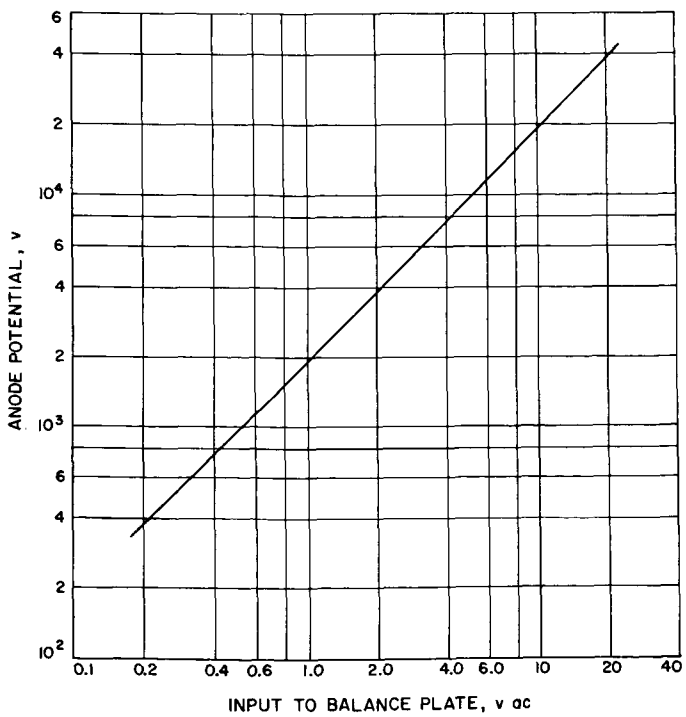

Fig. 16. Calibration curve for generating voltmeter

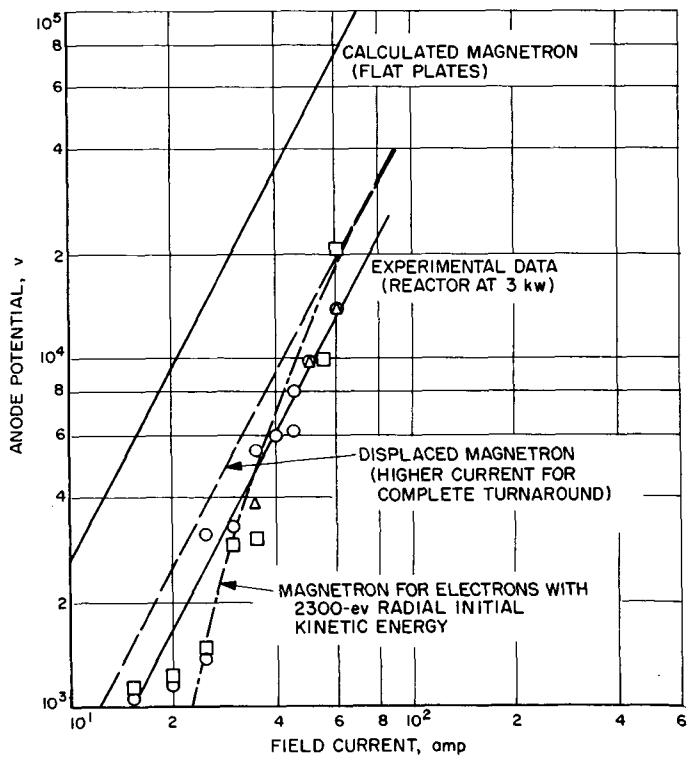

Fig. 17. Open-circuit potential as a function of magnetic field current, modified cell

limit curves for comparison. Maximum potential with no sweep ring voltage was in the range of 800 to 1000 v.

Reactor power level for this series of tests was 3 kw. At high power levels, the cell vacuum degraded under the large radiation fields, and results became erratic. At reactor power levels below 3 kw, the cell generated insufficient current to provide useful data.

During periods of cyclic charging and discharging of the cell, a slight increase in the ion-pump current accompanied each discharge. Eventually the vacuum degraded to a level at which voltage cycling stopped, and cell voltage stayed at the plateau value of 4000 $\pm$ 400 v. The vacuum would then improve and the cell would begin another cycle. The period between voltage peaks was from 5 to 10 sec.

The 21-kv peak noted above was the first after the cell had pumped for 3 days with no irradiation. The first several peaks determined after reactor start-up were 21 kv; however, the voltage peaks gradually decreased with cycling and then stabilized at the 13.5-kv value. Cell vacuum was gradually degrading during this period, and it too stabilized at the usual operating range of 3×10^{-8} mm Hg.

The magnetron equations used to determine the voltage capability of this cell configuration were determined by solving the differential equations of motion for plane geometry in Ref. 15. For the purpose of calculation, it was assumed that the cell could be approximated by the plane geometry case. With the assumption of no initial electron kinetic energy, and with the relativistic correction, the magnetron equation is:

$$B^2 = \left(\frac{2m_0}{e}\right)\frac{V}{S^2}\left[\frac{V}{m_0c^2/e} + 1\right]$$

where

B = magnetic flux

S = distance between electrodes $(r_c - r_a)$

m_0/e = mass-to-charge ratio of an electron

m_0c^2/e = rest-mass energy–to–charge ratio of an electron

V = potential between electrodes

With the assumption of an initial radial kinetic energy, the magnetron equation is:

$$\alpha = \frac{1 + (1 + \beta^2)^{1/2}}{\beta}$$

where

$\alpha = S\omega/v_i$ and $\beta = Bv_i\, S/V$

v_i = initial radial velocity of the electron

$\omega = B/m_0/e$

These equations are plotted in Fig. 17. An initial electron kinetic energy of 2300 ev was assumed.

VIII. DISCUSSION

It is possible to generate large electrical potentials using fission fragments. Magnetic field limitation of the present experimental apparatus limited the voltage of the cell to a small fraction of the voltage that the configuration appears capable of attaining. Although the potentials attained at the magnetic field strengths used were lower than the calculated magnetron-limit values, the experimental points follow a curve parallel to the calculated curves. This indicates that increased magnetic field would have resulted in increased cell voltage. The displacement of the experimental curve from the theoretical is believed due to uncontrolled end-effects.

During cell disassembly, uranium dioxide was found on the lower collimating ring of the cathode. It was also noted that there had been a high radiation level in this region, suggesting that the uranium was there during the irradiation period. Fragments generated in this region would produce electrons on which the magnetic field would have little effect, especially with an accelerating potential between the cathode and anode. In addition, fragment activity was found on the cell vacuum envelope above the anode interceptor. These fragments would also produce uncontrolled secondary electrons. The generation and collection of fission fragments in

regions of diminishing magnetic field would account for the increased field coil current required for complete electron turnaround under short-circuit conditions over that calculated, and would also explain the shift in the apparent magnetron cutoff potential of the cell under operating conditions.

The charging of the cell was cyclic, rather than steady as originally expected. This behavior could possibly be explained by examining the cell operation once the magnetron limit was reached. There were probably sufficient electrons in the space between the electrodes to constitute a space charge and to affect the potential gradient between the electrodes at potentials below magnetron cutoff. Once the electrode potential reached the magnetron limit and electrons started drifting to the anode, the potential gradient between the cathode and anode was altered so that confinement of the electrons was interrupted sufficiently to cause complete or at least partial discharge of the cell. This cyclic charging of the cell could probably have been overcome by matching an external load to the cell that would have limited the cell voltage to a value slightly below the peak value. In this way steady-state operation might have been attained and energy extracted from the cell. However, no provision was made for this type of cell operation.

It appears likely that the drift of electrons is the cause of the internal leakage current of a fission-electric cell device. Ideally, electrons that have originated at the cathode should, in the presence of a suitable magnetic field, be returned to the cathode. Any energy loss interaction that an electron may experience between the electrodes, however, will keep the electron from returning to the cathode. After losing energy, the electron will assume a new trajectory, and its closest approach to the cathode will depend on the amount of energy lost. In addition, it will approach closer to the anode and may even reach the anode. A most probable mechanism of energy loss is by ionizing collisions with the large number of neutral atoms sputtered by fission fragments. Electrons born as a result of any ionizing collisions will eventually drift to the anode since they cannot reach the cathode. The ions can produce additional sputtered material as they are accelerated into the cathode surface. The maximum probability for an ionizing collision with most atoms occurs at electron energies in a broad range around 100 ev. This means that ionizations probably occur primarily near the cathode where there is a high concentration of sputtered material.

Potentials required on sweep rings to ensure sufficient electron removal should be low compared with potentials that could be developed in a cell. Over the range of voltages developed in the cell, the required sweep potential was constant. This effect may be true for considerably higher cell voltages. As the voltage between the electrodes increases, the spatial volume where the ionization probability is large decreases. Thus, with increasing cell potential, the probability of an electron experiencing an ionizing collision decreases. Whether sweep rings could be eliminated at very large cell potentials is not known at this stage of experimentation; however, it can be assumed that the power requirements of such rings would be only a small fraction of the total cell output. Other means of electron removal may also be possible.

IX. CONCLUSIONS

The experiment has demonstrated the fission-electric cell concept and has indicated areas that must be pursued for the realization of a working device for the direct production of electrical energy from fission. The problem areas can be summarized as:

1. Handling of high voltages, with particular emphasis on insulators in radiation fields;
2. Electron and ion behavior in crossed electrostatic and magnetic fields, including effects of electrode geometries and sweep rings, as well as end effects;
3. Sputtering of material from electrodes by the high-energy fission fragments; and,
4. Fuel element material, including chemical form and treatment of the electrode surface before and after deposition.

REFERENCES

1. Safonov, G., *Direct Conversion of Fission to Electric Energy in Low Temperature Reactors*, RAND Corporation, RM-1870, 1957.
2. Safonov, G., *The Fission-Electric Cell Project (A Report on 1963 Operations)*, Final Report; Contract AT (04-3)-482, AEC-TID-20575, March 1964.
3. Shock, A., *A Direct Nuclear Electrogenerator—Analysis of Cylindrical Electrode Configuration*, AFOSR TN 59-590, Fairchild Engine and Airplane Corporation, Deer Park, New York, AD 216812, 1959.
4. Heindl, C. J., *Comparison of Fission-Electric Cell Geometries*, Technical Report No. 32-101, Jet Propulsion Laboratory, Pasadena, California, September 1, 1961.
5. Heindl, C. J., Krieve, W. F., and Meghreblian, R. V., "Fission-Fragment Conversion Reactor for Space," *Nucleonics*, Vol. 21, No. 4, p. 80, April 1963.
6. Krieve, W. F., and Heindl, C. J., *Fission-Electric Cell Capsule Experiment*, Jet Propulsion Laboratory, Pasadena, California, to be published.
7. Stein, W. E., and Leachman, R. B., "Fast Detector of Heavy Particles," *The Review of Scientific Instruments*, Vol. 27, No. 12, pp. 1049–1050, December 1956.
8. Lassen, N. O., "Energy Loss and Total Charges of Fission Fragments Passing Through Matter," *Proceedings of the International Conference on the Peaceful Uses of Atomic Energy, Vol. 2, Physics: Research Reactors*, p. 214–219, 1956.
9. Fulmer, C. B., "Equilibrium Charges of Uranium-235 Fission Fragments in Gases as Functions of Fragment Velocity, Gas Pressure, and Type of Gas," *Bulletin of the American Physical Society*, Vol. 2, p. 286, June 1957.
10. Dow, W. G., *Fundamentals of Electrical Engineering*, 2nd ed., pp. 104, 109, John Wiley and Sons, Inc., New York, 1952.
11. Bruining, H., *Physics and Applications of Secondary Electron Emission*, p. 37, Pergamon Press, Ltd., London, 1954.
12. Almen, O., and Bruce, G., "High Energy Sputtering," *1961 Transactions of the Eighth National Vacuum Symposium*, Vol. 1, October 16–19, 1961, Washington, D. C., The Macmillan Co., New York.
13. Smythe, W. R., *Static and Dynamic Electricity*, 1st ed., p. 491, McGraw-Hill Book Co., Inc., New York, 1939.
14. *American Institute of Physics Handbook*, pp. 7-174–7-182, ed. by D. E. Gray, McGraw-Hill Book Co., Inc., New York, 1957.
15. Dow, W. G., op. cit., p. 52.